Nylon 11/Silica Nanocomposite Coatings Applied by the HVOF Process. I. Microstructure and Morphology

E. PETROVICOVA,[1] R. KNIGHT,[1] L. S. SCHADLER,[2] T. E. TWARDOWSKI[1]

[1] Drexel University, Department of Materials Engineering, Philadelphia, Pennsylvania

[2] Rensselaer Polytechnic Institute, Department of Materials Science and Engineering, Troy, New York

Received 23 June 1999; accepted 9 November 1999

ABSTRACT: Nylon 11 coatings filled with nanosized silica and carbon black have been produced using the high velocity oxy-fuel (HVOF) combustion spray process. The physical properties and microstructure of coatings produced from nylon 11 powders with starting particle sizes of 30 and 60 μm have been evaluated as a function of the filler content, filler chemistry, and processing conditions. The nominal filler content was varied from 5 to 20 vol %. Co-milling of the nano-sized fillers with the polymer powders produced an embedded 4–8 μm thick filler layer on the surfaces of the polymer particles. Optimization of the HVOF processing parameters based on an assessment of the degree of splatting of polymer particles was accomplished by varying the jet temperature (via hydrogen/oxygen ratio). Gas mixtures with low hydrogen contents minimized polymer particle degradation. The filler was found to be agglomerated at the splat boundaries in the final coating microstructures. Aggregates of silanated silica and carbon black were of the order of 50 nm in size, whereas the aggregates of untreated silica and hydrophilic silica were of the order of 100 nm. The morphology of the polymer and the microstructure of the coatings depended on the filler surface chemistry and the volume fraction of the filler, as well as the initial nylon 11 particle size. Although all filled coatings had higher crystallinities than pure nylon 11 coatings, coatings produced from a smaller starting polymer particle size exhibited improved spatial distribution of the silica in the matrix and lower crystallinity. In addition, coatings prepared from smaller polymer particles had a higher density and lower porosity. © 2000 John Wiley & Sons, Inc. J Appl Polym Sci 77: 1684–1699, 2000

Key words: polymer nanocomposite; HVOF; thermal spray, nylon 11 coatings; composite microstructure

INTRODUCTION

Polymer coatings are used in an ever-growing range of applications, including surface protection against corrosion, weathering, and wear.[1] The use of polymer coatings in some applications is limited because of low scratch resistance, poor adhesion to metal substrates, or high coating permeability.

Polymer-based nanocomposites have attracted attention recently because they exhibit markedly improved physical properties compared to pure polymers or conventional microcomposites.[2–7] Sumita et al. demonstrated that 20 wt % of 7 nm silica reinforcement in semicrystalline nylon 6 increased the yield stress by 30% and Young's

Correspondence to: T. E. Twardowski.

Contract grant sponsor: National Science Foundation; contract grant number 9713650.

Journal of Applied Polymer Science, Vol. 77, 1684–1699 (2000)

modulus by 170% compared to pure polymers, while micron sized inclusions decreased the yield stress and only marginally increased the modulus.[2] They observed similar effects of nanosized fillers in polypropylene: dynamic storage modulus increased by almost 100% with the addition of 20 wt % of 7 nm silica particles while upon addition of the same amount of 200 μm glass particles dynamic storage modulus increased only by 20%.[3] Messersmith and Giannelis[4] reported that the dynamic storage modulus of layered mica-type nanocomposites containing 4 vol % silicate in an epoxy matrix increased by 58% in the region below the glass transition temperature and by 450% in the rubbery region. They also found[4] that the permeability of water in poly(ϵ-caprolactone) decreased by an order of magnitude with the addition of 4.8 vol % of mica-type silicate. Yano at al.[5] showed a 50% decrease in permeability for polyimide composites with as little as 2% mica content, while the thermal expansion coefficient was reduced by 25% compared to the bulk polymer.

An important technical challenge, however, in the practical use of nanocomposite coatings is achieving a uniform dispersion of the nanoparticulates within the polymer matrix because of the high viscosity of composite melts.[6,7] Processing requires either large amount of solvent (20 to 60 vol %)[6] or high processing temperatures or *in situ* polymerization.[7] Filler volume, particle morphology, and size have the most important effect on the viscosity of filled polymer melts. Deviations from spherical shapes result in increased interparticle interactions, while smaller particles have a higher tendency to agglomerate, both effects causing an increase in viscosity. Recent restrictions on paints and solvents containing volatile organic compounds (VOCs) by the Environmental Protection Agency also accentuates the need for environmentally acceptable alternatives to solvents for the application of organic coatings and paints.

Thermal spray is an excellent solution for overcoming the processing limitations of other coating application techniques. Thermal spray, in general, is a process in which a material, in powder, wire, or rod form, is heated, accelerated and propelled by a high temperature jet through a confining nozzle toward a surface. The individual molten or softened droplets impact, spread (usually called "splatting"), cool, and solidify to form continuous coatings. Particle heating, quenching, consolidation and post-treatment are thus combined into a single step process in which relatively thick coatings (up to several millimeters) can be produced.[8]

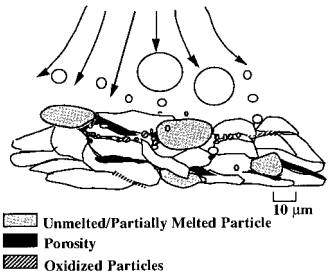

Figure 1 Schematic of coating deposition, depicting the major microstructural features generally found in thermal spray coatings.

The important benefits of using a thermal spray process for the application of polymer nanocomposite coatings include: (a) application of coatings with high melt viscosity.[8] Materials are processed in the form of powders and heated only to a temperature at which the particles are viscous enough to spread on impact at the surface due to the high kinetic energy. (b) processing without use of volatile organic solvents, eliminating the need for costly solvent removal. (c) coating large substrates under almost any environmental condition (such as the coating of a bridge reported by Brogan[9]), the application and repair of these coatings outside the laboratory and a large range of coating thicknesses (from a few μm up to several mm).

The schematic in Figure 1 illustrates the major microstructural features generally found in thermal spray coatings. These include melted, partially melted, and unmelted particles, oxidized particles, and porosity. Heated particles/droplets become flattened, disc-like structures ("splats") upon impact, which spread over the substrate surface and fill underlying interstices. At impact, particles from all positions in the jet, with varying degrees of melting, deposit continuously to form the coating. If the particles are not fully molten upon impact, then coatings characterized by a "cell structure" of matrix particles can be produced. Solid particles do not flow easily on impact, and will not conform fully to underlying surface asperities, thus creating porosity in the coating. An optimum balance between sufficient heating without in-flight degradation must be determined.

Plasma and flame spraying are currently used for polymer coating applications. Plasma, com-

bustion (including flame and high velocity oxy-fuel) and wire-arc spraying constitute the major thermal spray processes. Thermal heating is supplied either from electrical (plasma) or chemical (combustion) sources. Microstructural properties of thermal sprayed coatings can be manipulated using numerous spray parameters. Specifically, dwell time and jet temperature determine the degree to which materials are heated, and are controlled by jet velocity and gas heating. Spray distance, the powder injection location and the position of the coated part also influence particle temperature. These, in turn, affect the splatting behavior and degradation of the material.

Materials that have been deposited include: polyetheretherketone (PEEK) and polyphenylenesulphide (PPS),[10, 11] polyethylene terephtalate (PET),[12,13] polyester (PES) and polyethylene (PE),[14–18] polyvinylidene fluoride (PVDF),[15,16] polypropylene (PP),[17] polycarbonate (PC), polysulfone (PSF),[18] polyamides,[15–17,19] polymethylmethacrylate (PMMA),[20] and polytetrafluorethylene (PTFE) and its copolymers.[15,17,18] There have been some reports on spraying composites, mainly micron-sized filled polymers, including Al_2O_3, SiO_2-filled epoxy,[21] Al_2O_3, and NiCr-filled EMMA,[22] glass, Al_2O_3, SiO_2-filled nylon 11.[20] Filler dispersion was reported to be a strong function of the powder injection angle and the filler size. Layered structures were obtained when the polymer powder was injected at 90° to the plasma jet.[23] Several authors reported that a more homogeneous filler distribution was achieved when the powder was injected at 45°.[20,24] Lower filler deposition efficiency was observed in the case of larger fillers (>60 μm), especially in the layers next to the substrate.[25]

There have been only a few studies reported on spraying of polymers using high velocity combustion spraying (HVOF).[10,13,26,27] In HVOF, thermal energy for heating is provided by combusting fuels with oxygen. The spray conditions for polymers differ significantly from those typically used for metals and ceramics. In previous work[27] we showed that the lower jet temperatures, up to 2500°C, obtained using the HVOF combustion spray process, provided better control of particle heating without requiring equipment modifications. Lean gas mixtures, (hydrogen/oxygen ratios between 0.36–0.45), shorter spray distances (0.2 m), and high total gas flow (up to 17×10^{-3} m^3 s^{-1}) were found to be optimal for processing. Solution viscometry has confirmed that the HVOF spray parameters chosen do not result in significant polymer degradation.[27] Furthermore, the high particle velocities achieved in the HVOF process, around 1000 m s^{-1}, depending on the particle density and size,[28] are significantly higher than in conventional flame spraying (50–100 m s^{-1}) and higher than those achieved in plasma spraying (up to 800 m s^{-1}). Higher particle velocities and lower jet temperatures result in higher coating densities, improved adhesion and, because of large particle deformations on impact, more uniformly dispersed coating structures.[28]

In this study, we concentrated on characterization and understanding the changes that nanoreinforced polymers underwent during thermal spraying, and how these changes affected the final polymer morphology and coating performance. Detailed microscopic studies of nanosized filler dispersion and distribution along with coating thermal properties and crystalline content are presented. Throughout, we will use the term microstructure to refer to filler dispersion and distribution, and to splat shape and size. The term morphology will refer to the general molecular arrangements within the polymer, including crystallinity.

EXPERIMENTAL

Materials

Nylon 11 powders with mean particle sizes of 30 and 60 μm (designated as nylon 11 D-30 and nylon 11 D-60, or D-30 and D-60, respectively) were chosen as the matrix material. Nylon 11 exhibits high chemical resistance and a wide processing window—melting at ~183°C and degrading at much higher temperatures (~360–550°C). Nylon 11 has also been widely used as a coating because of its combination of low-temperature flexibility, low friction coefficient, high mechanical strength, and chemical resistance. Examples of demanding applications include pipework and tubing,[29] printing rollers and splined drive shafts,[30] airport luggage trolleys, outdoor furniture, and marine hardware such as boat ladders and diving tanks.[31]

The two most commonly used polymer fillers—silica and carbon black—were selected as nanoreinforcement. These are found in products ranging from paints and printing inks,[32] tires,[33] polymer composite materials used in aircraft, and comput-

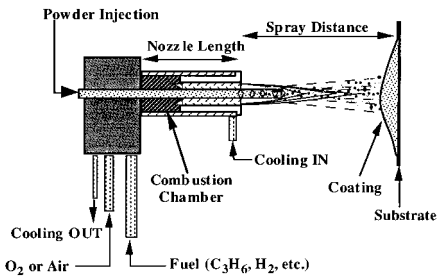

Figure 2 Schematic of the HVOF (Jet Kote II®) process.

ers,[34] to personal items such as protective helmets and utensils.[35] They are used both as pigments and for their reinforcing properties.

Seven- and 12-nm size silica powders ("R 812" and "A 200" contributed by Degussa Corporation) with hydrophobic and hydrophilic surface chemistries, silanated "R 812 silica," and 6-nm size carbon black (also from Degussa Corporation) were used as nylon 11 reinforcement. To vary the interaction of the polymer with the silica particles, the silica surface chemistry was modified using A 1100 gamma-aminopropyltriethoxy silane, referred to as "silanated silica." Silanes are applied to decrease or remove hydrophilic properties of silica surface and to reduce agglomeration. Through silane treatment, new organofunctional groups with higher chemical affinity to specific polymers can be incorporated on the SiO_2 surface.[36] Silica was mixed for 3 h in a silane–toluene solution, and dried at a temperature 105°C to remove the solvent. To ensure uniform wetting of the filler surface the amount of silane was kept at 5% by weight of silica in toluene.

Co-spraying two powders can result in significant powder segregation in the jet due to differences in powder size and density. Powders were prepared for spraying by dry ball-milling nylon 11 ("French Natural ES" contributed by Elf Atochem North America, Inc.) together with the nanoparticulate phase for 48 h in a Norton Ball Mill using zirconia balls to create a composite powder. The composite powder aids both in distribution of the filler in the coating and in simultaneous powder feeding into the HVOF spray jet.

The nominal volume fraction of filler in the powder compositions sprayed ranged from 5 to 20 vol %. Except where noted, the samples are referred to according to the nominal volume percent of filler in the starting materials.

Coating Procedure

A Stellite Coatings Jet Kote II® HVOF (Fig. 2) combustion spray gun with internal powder injection and a 76 mm (3″) long by 8 mm (5/16″) diameter nozzle, was used to spray the polymers. Optimal powder feed rate, carrier gas flow, gun motion, and spray distance have been evaluated previously,[27] and kept constant at these values, summarized in Table I. Additional optimization was accomplished as summarized in Tables II and III. Tables II and III also list the adiabatic flame temperatures, estimated according to the method of Chomiak,[37] described in the Results section.

The nano-sized silica-reinforced nylon 11 composites were deposited onto 25.4 × 75.2 × 3 mm (1″ × 3″ × 0.125″) aluminum (6061) coupons. Prior to spraying, the substrates were grit blasted using 1600-μm size SiC grit and cleaned in ethanol in an ultrasonic bath. Coatings for subsequent thermal and structural analyses were sprayed onto polished aluminum substrates to allow for easy removal of the coating. The substrates were preheated to approximately 80°C by traversing the HVOF jet over the substrate surface before powder injection. Typical coating thickness was between 250–350 μm (0.014 in).

Coating Characterization

The filler contents of the sprayed composite coatings were determined using a DuPont model 951 thermal gravimetric analyzer (TGA), by weighing the residue after complete ashing of the coating at 800°C in dry air. Reported values represent the

Table I HVOF Spray Parameters Which Were Kept Constant in This Study

Powder feed rate	0.25 g s^{-1} (15 g min^{-1})
Powder carrier gas	Nitrogen
Powder carrier gas flow	0.5×10^{-4} m^3 s^{-1} (60 scfh)
Powder carrier gas pressure	0.97 MPa (140 psi)
Sample velocity	Stationary
Gun surface speed	0.23 m s^{-1} (45 ft min^{-1})
Step size per pass	3.2×10^{-3} m (0.125 in)
Spray distance	0.2 m (8 in)

Table II Spray Parameters Used for Deposition of the Nylon 11 D-60 Nanocomposite Coatings Reinforced with: (a) Hydrophobic Silica, (b) Hydrophilic Silica and (c) Carbon Black Filler

Nominal Filler Content (vol %)	Total Gas Flow Rate at 0.83 MPa (10^{-3} m^3 s^{-1})	Hydrogen/Oxygen Ratio	Estimated Adiabatic Flame Temperature (°C)
(a) Hydrophobic silica			
0	15.7	0.36	1930
5	15.3	0.37	1966
10	15.3	0.38	1990
15	16.1	0.42	2115
20	16.6	0.45	2192
(b) Hydrophilic silica			
0	15.7	0.36	1930
5	16.1	0.39	2027
10	16.3	0.41	2082
15	16.6	0.43	2134
20	17.0	0.50	2291
(c) Carbon black filler			
0	15.7	0.36	1930
5	16.1	0.42	2115
10	15.7	0.41	2082
15	15.7	0.38	1989
20	16.2	0.42	2115

mean of three measurements taken from different locations on the coated substrates.

The distribution of the reinforcement and the coating microstructures were studied by optical, scanning and transmission electron microscopy. Samples were mounted in a slow curing epoxy and an exposed coating cross-section was then polished using SiC papers. The phase composition of the coatings was determined by energy dispersive X-ray spectroscopy (SEM-EDX) on gold-coated coating cross sections. To clearly distinguish the filler particle agglomerate sizes the SEM samples were etched using an oxygen plasma for 3 min prior to gold coating.

The density of the coatings was measured according to ASTM D 792-91,[38] by weighing the sample in air (w_{air}) and in kerosene (w_{fl}). Sample density was then calculated according to eq. (1):

$$\rho = \frac{w_{\text{air}}}{(w_{\text{air}} - w_{fl})/\rho_{\text{kerosene}}} \quad (1)$$

Density values represent the mean of three measurements, reported in kg/m^{-3}.

Table III Spray Parameters Used for Deposition of Nylon 11 D-30 Coatings Reinforced with Hydrophobic and Hydrophilic Silica

Nominal Filler Content (vol %)	Filler Type	Total Gas Flow Rate at 0.83 MPa (10^{-3} m^3 s^{-1})	Hydrogen/Oxygen Ratio	Estimated Adiabatic Flame Temperature (°C)
0		14.9	0.29	1725
10	hydrophilic	16.1	0.41	2082
15	hydrophilic	16.6	0.43	2134
10	hydrophobic	16.1	0.38	1990
15	hydrophobic	14.9	0.42	2115

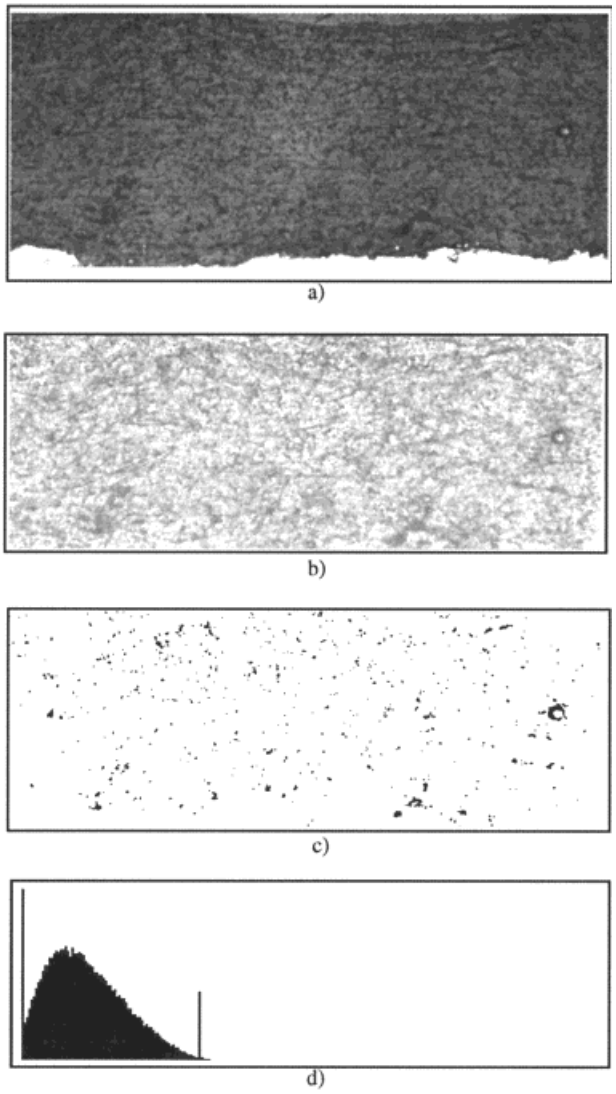

Figure 3 Porosity evaluation on cross section of nanocomposite coating: (a) optical image of nanocomposite coating at 100× magnification, (b) image background subtracted by 2-D rolling ball averaging, (c) image with threshold level determined from (d) histogram and color density (porosity appears black on the image).

Coating porosity was determined from optical images of the coating cross sections using NIH Image Analyst 1.41 software, as illustrated in Figure 3. A two-dimensional rolling-ball filter was used for background subtraction. Using the gray-scale density histogram, a threshold value was established for the porosity as the point where the Gaussian distribution increase became nonlinear, as shown in Figure 3(d). The porosity is depicted as black in the image of Figure 3(c). The silica-rich and polymer-rich areas were determined as gray and white on the image, the division between the two being drawn from the peak intensity in the histogram. Porosity content was calculated by comparing the black and the image areas. Results were the mean of nine measurements taken at three different coating cross sections.

A Siemens model D-500 Diffraktometer was used to obtain X-ray diffraction patterns. Fractional crystallinity was estimated using the 5 to 35° (2Θ) range of the diffraction intensity curves by comparing the integrated intensities for each composite system to the total integrated area of an amorphous nylon 11 sample.[39] This amorphous sample was prepared by rapidly quenching melted pure polymer in liquid nitrogen.

Crystallinity was also determined using DSC. The heat of fusion was measured using a Perkin-Elmer model DSC-7 differential scanning calorimeter (DSC) at a heating rate of 20°C min^{-1} in dry nitrogen. Crystallinity was calculated by comparing the heats of fusion of sprayed coatings to starting powder with the manufacturer reported value of 21% crystallinity. Data reported are the mean of three measurements.

Fourier transform infrared spectroscopy (FTIR) was used to characterize polymer degradation. FTIR spectra of the coatings and the original powders were obtained using a Magna model 560 FTIR spectrophotometer.

RESULTS AND DISCUSSION

Coating Microstructure

Dry ball-milling mechanically embedded the smaller filler particles into surface layers on the nylon powder particles, rather than uniformly distributing the filler within the polymer particle. Figure 4(a) and (b) shows typical nylon 11 D-60 powder particles after ball milling with nominal 5 and 15 vol % silica, respectively. The thickness of the embedded silica layer on the surface of the nylon particles varied from 4 to 8 μm for nominal 5 and 15 vol % filler contents, respectively. Filler particles can be held to the surface by electrostatic forces or embedded by mechanical interlocking. As the outer surface of the polymer particle is hardened by the filler, it becomes difficult to embed more filler. This may limit the amount of filler that is effectively bound to the polymer surface.

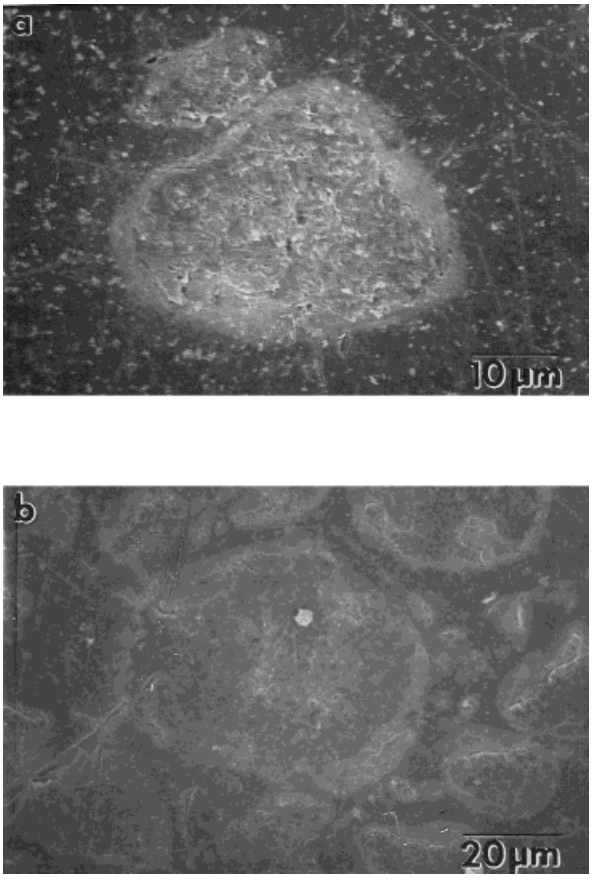

Figure 4 SEM micrographs of powder particles after ball milling of (a) 5 and (b) 15 nominal vol % of hydrophobic silica with nylon 11 D-60.

Table IV shows the actual filler contents in nanocomposite coatings compared with the nominal filler content in powders. The residual filler content in the coatings produced from both nylon 11 D-30 and D-60 were similar for untreated silica, in the range from 2.4 to 6.9%. The residual content of silanated silica and carbon black in D-60 coatings, however, was approximately 1–2% higher than this. Ball milling of polymer powder with nominal 20 vol % filler did not result in a significantly increased filler content in the coating compared to the nominal 15 vol %. A 7.7 vol % of silanated silica and 10.3 vol % of carbon black was the maximum filler content achieved in thermally sprayed coatings.

The composite coatings had ca. 50% lower filler contents in all cases than the starting powders. Layered particles are carried by the high velocity moving jet and are impacted at the substrate by high kinetic force. Poorly bound particulate fillers may have been lost during spraying or at impact.

The benefits of mechanical milling included improved feeding of the powder into the thermal jet and safer handling of silica powder. Difficulties with powder flow, such as nozzle clogging and irregular flow, during spraying of pure polymer powders were reduced by the addition of the nanosized filler. The presence of filler particles on the polymer particle surfaces reduced the agglomeration of polymer particles observed to cause these problems. It also improved the handling of silica powder during spraying.

The morphology of the coatings and the resulting coating properties depend on the thermal profile and heating of the powder. To avoid any polymer degradation during the spray process, the temperature of the thermal jet was carefully controlled using a very lean combustion flame, with excess oxygen used in the gas mixture to decrease the thermal mass of the gas and reduce the adiabatic flame temperature. For a stoichiometric ratio of hydrogen/oxygen (2 : 1), the flame temperature is reported to be 2856°C.[40] The adiabatic flame temperatures of the gas mixtures used in this work were in the range of 1800–2400°C, depending on the hydrogen/oxygen ratio, and are

Table IV Nominal vs. Actual Filler Contents in Composite Powders and Filled Nylon 11 D-30 and D-60 Coatings

Nominal Filler Content in Powder (vol %)	Silica in D-60 Coatings (vol %)	Silanated Silica in D-60 Coatings (vol %)	Silica in D-30 Coatings (vol %)	Carbon Black in D-60 Coatings (vol %)
5	2.4	3.2	—	4.9
10	4.5	6.2	4.6	7.1
15	6.7	7.7	6.9	10.3
20	6.9	—	—	10.1

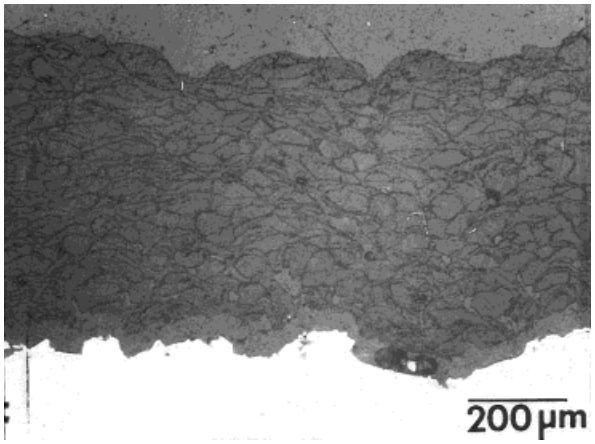

Figure 5 Optical micrograph of nanocomposite coating with nominal 10 vol % of hydrophobic silica filler prepared from nylon 11 D-30 showing significant cell structure.

listed in Tables II and III. These were estimated according to the method of Chomiak[37] from:

$$\sum_{i=1}^{P} n_i \int_{298}^{T_f} c_{pi}\, dT = \sum_{j=1}^{R} n_j \Delta H_{fj} - \sum_{i=1}^{P} n_i \Delta H_{fi} \quad (2)$$

where $n_{i,j}$ are numbers of moles of i, j present in the system before and after reaction, respectively, $\Delta H_{F,j,i}$ are the heats of formations of reactants (R) and products (P), c_{pi} are specific heats of products and T_F is the adiabatic flame temperature. This is an adiabatic model that assumes that all the heat generated remains within the system, giving rise to an increase in temperature. The endothermic effects of dissociation products were not considered, because they are not significant for temperatures up to 2300–2400 K or in lean mixtures.[37]

Further control of the heat input to the particles was regulated by dwell time in the high temperature jet. Time was minimized by using a short spray nozzle [0.076 m (3″)]. The effect of the nozzle length was reported in previous work.[27]

The optimal gas composition and flow rates for each powder composition were determined using an optical microscopic evaluation of the corresponding coating. It was necessary to "fine tune" the jet temperature for each filler content. Increased total gas flow and lower hydrogen contents in the gas mixture were determined to be necessary for pure nylon 11 D-30 powder deposition to obtain coatings without significant polymer degradation (Table III) compared to D-60 and composite powders. As shown in Tables II and III, increasing amounts of filler required increased jet temperatures, reflected by an increase in fuel gas (hydrogen) content, as expected, due to the increase in thermal mass. Hydrogen contents in excess of 50% resulted in jet temperatures that caused degradation of the coatings, with an obvious change in color to light tan or dark brown, and spalling of the coating at the edges or complete debonding of the coating from the substrate after cooling. Hydrogen contents below 30%, with jet temperatures up to 1725°C for D-30 and up to 1930°C for D-60 polymer, produced more friable coatings with significant cell structure and low interparticle cohesion, as shown on Figure 5, where some unmelted/partially melted particles are visible. This implied that the powder particles were insufficiently melted to allow the required splatting and coalescence. An optimized jet temperature, which depends on particle size and filler content and ranged from 1725–2115°C, resulted in improved splatting. This was confirmed by the observation of highly deformed, smaller cells. In general, smaller particles of nylon D-30 seemed to be heated faster than the larger nylon 11 D-60 and composite particles, which again is consistent with the increased thermal mass.

The infrared spectra of sprayed nanocomposite nylon 11 coatings are shown in Figure 6. It was reported that the high temperature degradation of nylon 6 and 6,6 polymers takes place by chain scission at the —NH—CH_2— bonds, and it is likely that a similar mechanism occurs in nylon 11.[41] Carbonamide and unsaturated hydrocarbons are typical products of chain scission, indicated by an intensity reduction of the bands at

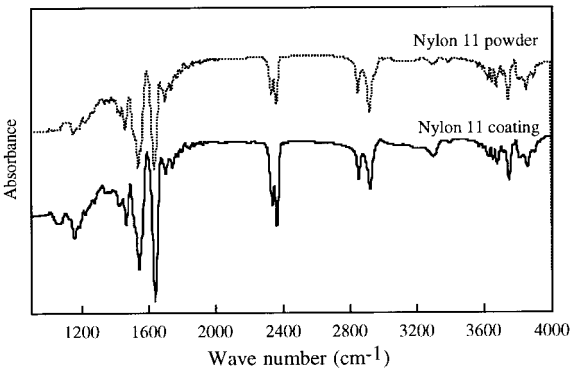

Figure 6 Fourier transform infrared spectra of nylon 11 D-30 powder and nylon 11 D-30 sprayed coating.

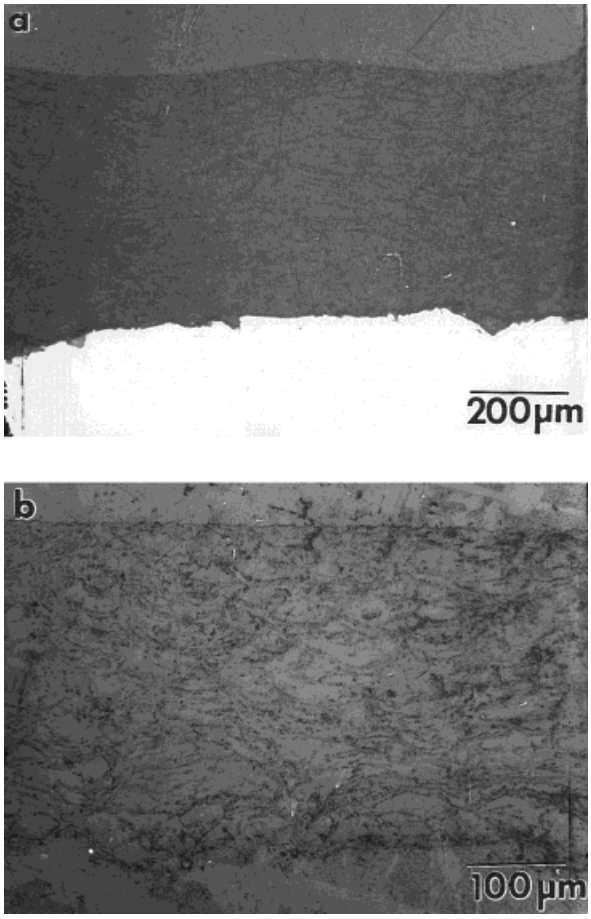

Figure 7 Optical micrographs of nanocomposite coatings with nominal 10 vol % of hydrophobic silica filler, prepared from nylon 11: (a) 30 μm and (b) 60 μm mean powder particle size.

1546 cm^{-1} and 721 cm^{-1}. During further degradation other products can form, for example, carbonitriles, the presence of which was confirmed by the stretching vibration at 2244 cm^{-1}, and their end groups can interact in a number of ways to produce simple gaseous compounds including CO_2 and H_2O.[42] FTIR analysis did not reveal the presence of any degradation products, nor did it reflect any significant differences between pure and sprayed nylon.

It was anticipated that the use of a finer starting powder, 30 vs. 60 μm, would result intrinsically in a more homogeneous distribution of the reinforcing phase owing to three factors: (1) the smaller initial polymer domain size, (2) the high kinetic energy of the HVOF spray process, and (3) the typical microstructural development of thermal sprayed coatings. Figures 7(a) and (b) show the microstructure of HVOF sprayed nylon 11 coatings produced from polymers of different particle sizes (30 and 60 μm) with nominal 10 vol % silica contents. Highly deformed, disc-like splatted particles with uniform distributions in both types of coatings indicated that optimal jet temperatures were achieved, resulting in good "in-flight" melting and high deformation of the particles on impact. The dark lines are silica rich layers "embedded" between splatted polymer particles as will be discussed below.

As expected, in the case of coatings produced from the smaller feedstock powders, the coatings possessed a finer "cell" structure. Therefore, an improved spatial distribution of the silica was observed [Fig. 7(a)] compared to coatings prepared from powders with 60 μm nominal particle size [Fig. 7(b)]. However, a cell structure did persist in the D-30 microstructure.

SEM-EDS elemental dot mapping of "cell structure" coatings confirmed that the reinforcing phase embedded in the surface of the nylon particles during ball milling remained agglomerated after spraying at the edges of cell domains having approximately the same volume as the original polymer particles [Fig. 8(a)]. As shown in Figure 8(b), the internal "cell" areas consisted almost entirely of nylon 11 elements (carbon, hydrogen, oxygen, and nitrogen), with traces of silica only evident in the spectrum of the surrounding cell "wall."

Also important was the dispersion of the individual silica particles, which was difficult to mea-

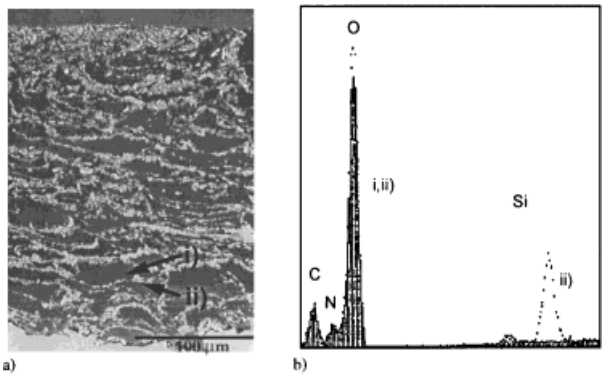

Figure 8 (a) An SEM image of the coating showing clearly defined regions. with (i) a "cell" composed of a polymer-rich region, and (ii) a silica-rich interface. This is confirmed by (b) the EDS element spectrum, which show silica to be present only in the interface regions. (i: (—) "cell" region, ii: (---) interface).

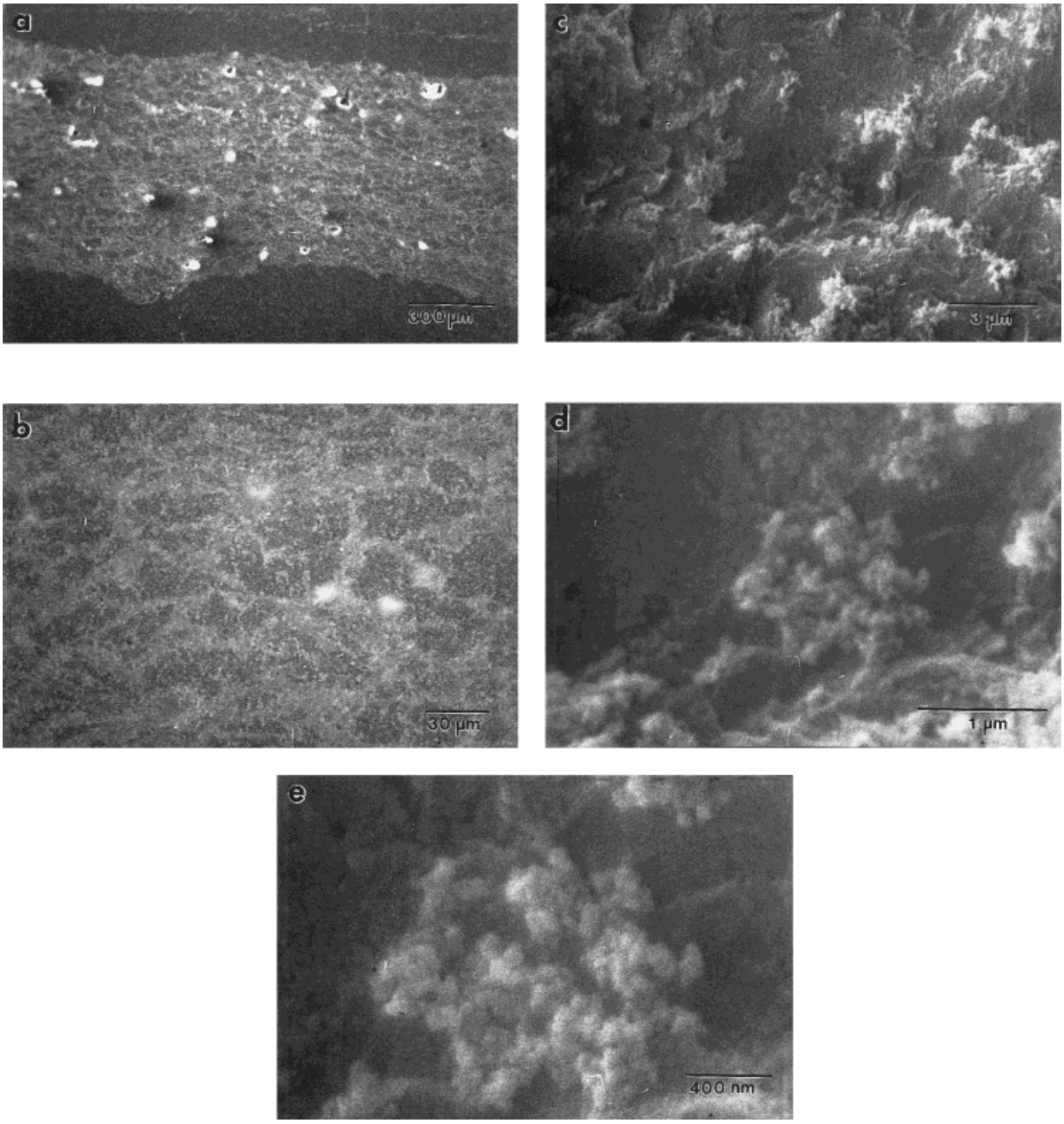

Figure 9 Scanning electron micrographs of the nylon 11 D-60 coating microstructure filled with nominal 10 vol % of silanated silica particles at various magnifications: (a) 65×; (b) 325×; (c) 6500×; (d) 19,500×; and (e) 32,500×. Samples were etched by O_2 plasma for better visualization of silica particles.

sure and control. An improvement in the dispersion and spatial distribution of silanated silica in thermal sprayed coatings was observed as shown in the detailed SEM micrographs. Figures 9(a) and 10(a) are SEM micrographs of nylon 11 D-60 and D-30 coatings reinforced with 10 vol % of silanated and untreated silica, respectively, showing the area of the coatings further enlarged in Figure 9(b)–(e) and Figure 10(b)–(e) for clarity. Using the smaller powder particle size the polymer rich "cell" areas were reduced compared to coatings of nylon 11 D-60 [Fig. 9(b)] with larger polymer-rich areas clearly visible in the coating cross section. There appeared to be thinner and

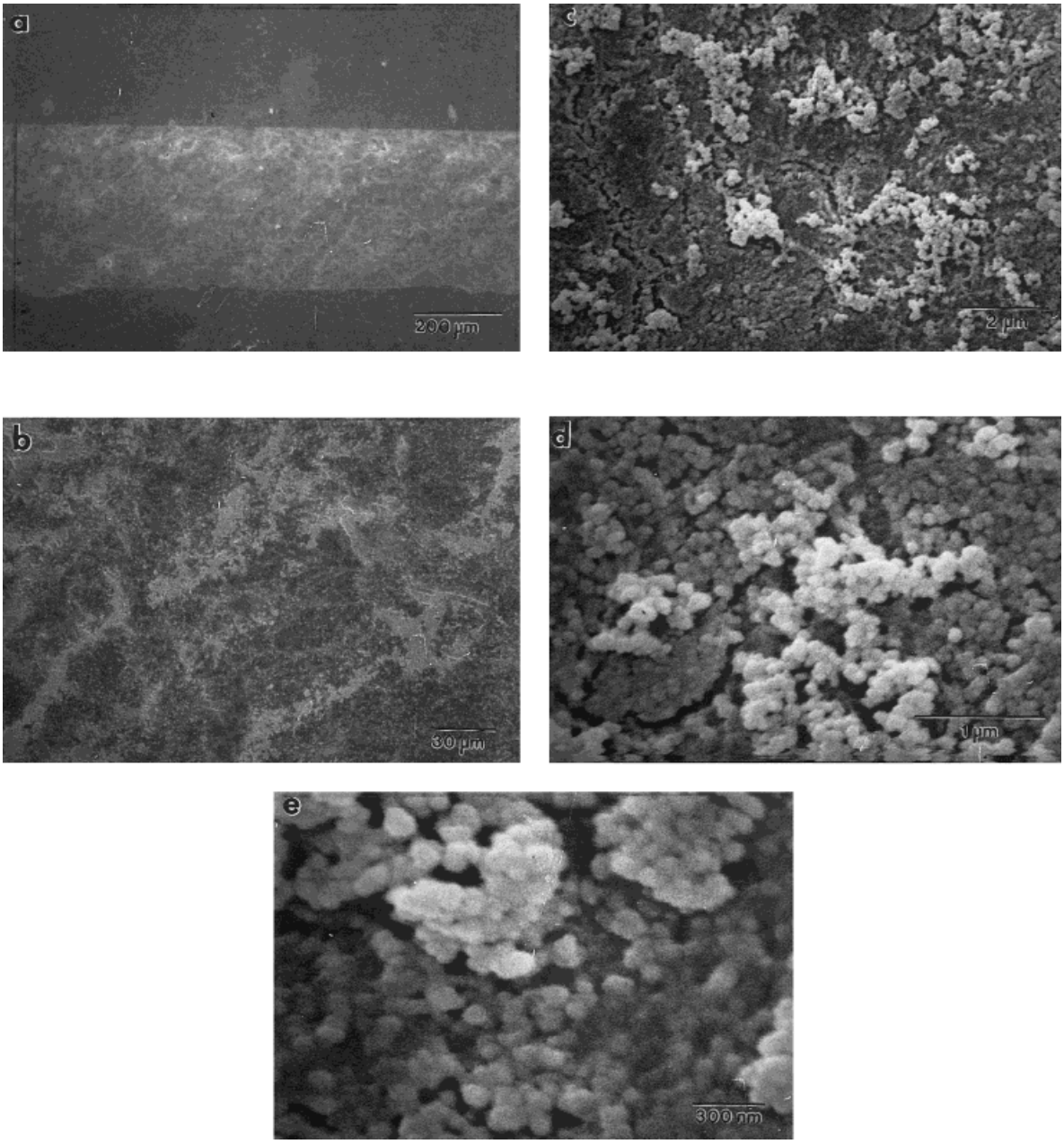

Figure 10 Scanning electron micrographs of the nylon 11 D-30 coating microstructure filled with nominal 10 vol % of untreated silica particles at various magnifications: (a) 65×; (b) 325×; (c) 6500×; (d) 19,500×; and (e) 32,500×. Samples were etched by O_2 plasma for better visualization of silica particles.

gradual transitions from the silica-rich areas to the nylon-rich areas in the silane treated material [Fig. 9(c)], where filler layer thickness varied between 1–5 μm, compared to untreated silica [Fig. 10(c)] where a sharp transition between the two materials were observed. The average filler layer thickness was measured between 2–6 μm. The agglomerates of untreated silica [Fig. 10(d) and (e)], appeared to be on the order of 50 nm or larger, while they were on the order of 20 to 50 nm in silanated coatings [Fig. 9(d) and (e)]. Smaller particle agglomerates, in the range between 50–70 nm, were also observed in carbon black filled composites (Fig. 11). This was probably due

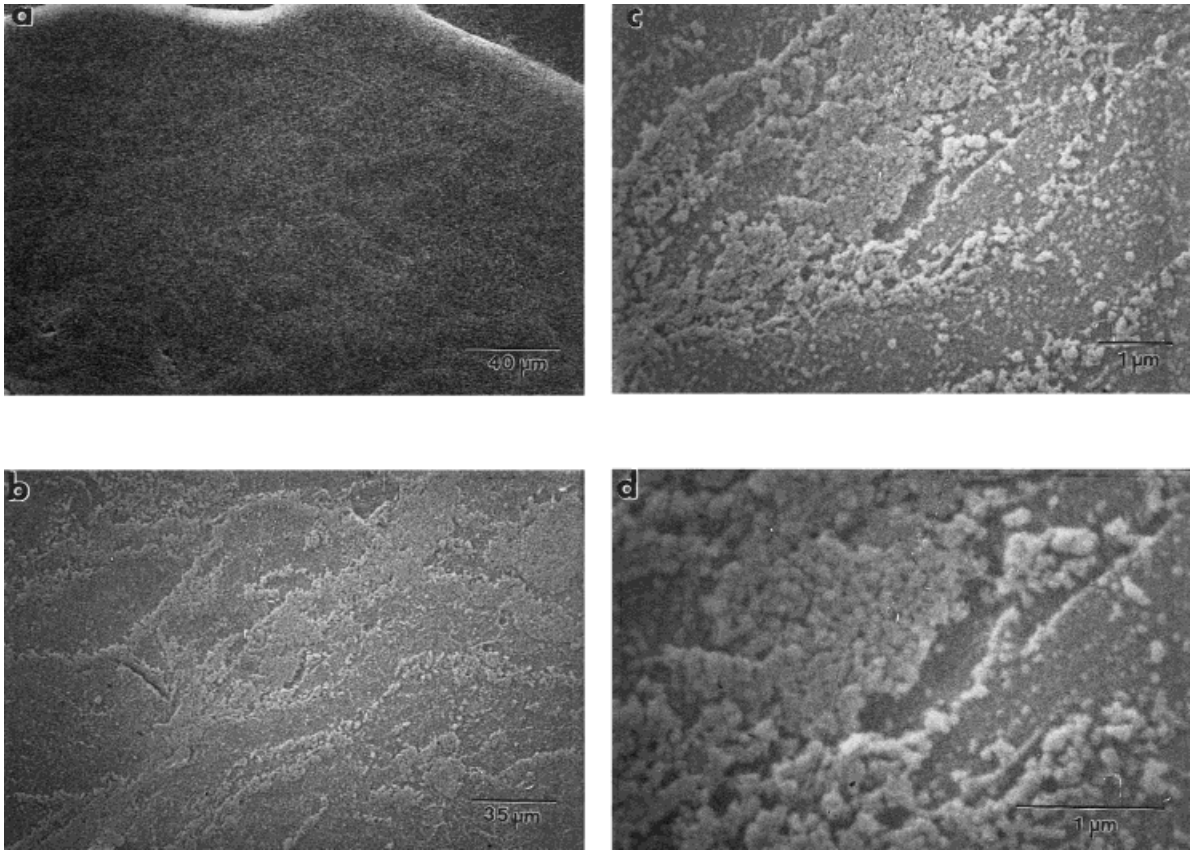

Figure 11 Scanning electron micrographs of the nylon 11 D-60 coating microstructure filled with nominal 10 vol % of carbon black at various magnifications: (a) 325×; (b) 9750×; and (c) 19,630×. Samples were etched by O_2 plasma for better visualization of the silica particles.

to both a lower affinity between the carbon particles and the polymer and to reduced electrostatic forces between the particles.

The densities and porosities of various coating types are summarized in Table V. Coatings produced from the smaller particle size powder (D-30) were found to be both denser and to have lower porosity content than those produced from the polymer with larger particle sizes. The density values of D-30 were in the range between 1.1 up to 1.3 g/cm^{-3} compared to 1.1 up to 1.2 g/cm^{-3} for D-60 coatings. Porosity content was measured

Table V Density and Porosity of D30 and D-60 Nylon 11/Silica Thermal Sprayed Nanocomposite Coatings

Silica Content (nom vol %)	Silica Surface	Density D-30 (10^{-3} kg m^{-3})	Density D-60 (10^{-3} kg m^{-3})	Porosity D-30 (%)	Porosity D-60 (%)
0		1.12	1.1	1.46	1.82
10	Hydrophobic	1.3	1.16	0.65	0.93
15	Hydrophobic	1.32	1.18	0.5	0.86
10	Hydrophilic	1.27	1.16	0.45	0.74
15	Hydrophilic	1.3	1.2	0.41	1.15

Table VI Heat of Fusion ΔH of D-30 and D-60 Thermal Sprayed Nanocomposite Coatings

Nominal Filler Content (vol %)	Filler Type	Coating Matrix	ΔH [J/g_{nylon}]	Crystallinity Content[a] (%)
0		Powder D-60	87.3	21
0		D-60	54.2	13
0		D-30	51.8	12
10	Hydrophobic silica	D-60	63.8	15
10	Hydrophilic silica	D-60	57.5	14
10	Hydrophobic silica	D-30	57.7	14
10	Hydrophilic silica	D-30	54.5	13
15	Hydrophobic silica	D-60	60.0	14.5
15	Hydrophilic silica	D-60	58.7	14
15	Carbon black	D-60	75.4	18
15	Hydrophobic silica	D-30	57.6	14
15	Hydrophilic silica	D-30	54.9	13

[a] Assuming 21% crystallinity of starting powder as reported by the manufacturer.

from 0.5 up to 1.5% for D-30 coatings compared to 0.7 up to 1.9% of D-60 coatings. Density can be affected by porosity, filler content, and crystallinity. Density in thermal sprayed coatings increased with reduced porosity in the D-30 coatings more than in the D-60 coatings with corresponding filler content. It is believed that smaller sized polymer particles were heated more homogeneously, thus improving polymer flow on impact, resulting in better filling of the interstices on the underlying substrate and between particles in the underlying coating layers. Because the nylon D-30 coatings had lower crystallinity contents than D-60 coatings, as discussed below, it is therefore believed that the higher density of D-30 coatings was mainly the result of decreased porosity.

Crystallinity

The effect of filler content on coating crystallinity was evaluated by DSC and X-ray diffraction. The results of DSC analysis are summarized in Table VI. All nanocomposite coatings exhibited an increased heat of fusion relative to pure polymer coatings. All values were also lower than the heat of fusion of the pure nylon 11 powder, which corresponded to 21% crystallinity, giving a ΔH of 87.3 J/g_{nylon}. A lower crystallinity content in the sprayed coatings than in the starting powder is typical for thermal spray processes due to the high cooling rates and short post-deposition fusion creating a tendency towards quenching.[13,43]

The largest increase in heat of fusion relative to the unfilled coatings was measured for the hydrophobic silica with nominal 10 and 15 vol %, representing 15 and 14.5% crystallinity contents and for carbon black filled coatings with nominal 15 vol % filler content, representing an 18% crystallinity, in D-60 composites. The heats of fusion for the composite of nylon 11 D-60 coatings increased by 6–40% relative to pure nylon 11 coatings, which was attributed to the presence of the filler particulates. Filler can initiate heterogeneous crystallization and change the thermal characteristics of polymers.[44] Crystal content positively affected the coating properties as will be discussed in the following publication.

The heats of fusion were typically higher for coatings prepared from the nylon 11 D-60 polymer matrix compared to nylon 11 D-30 coatings. The lowest crystallinity content, 12%, was measured in pure nylon D-30 coatings. It was proposed that the original crystallites were fully remelted in the smaller powder particles and the high cooling rate did not allow sufficient time for higher degrees of crystallization to be achieved. Due to the filler effect, the crystallinity content was higher in D-30 filled coatings relative to pure D-30 coatings, but despite the presence of the filler the crystallinity content did not reach the levels exhibited by D-60 composite coatings.

In addition to DSC, coating crystallinity contents were also determined using X-ray diffraction. Figure 12 shows typical X-ray diffraction curves, with characteristic peaks at the 21 and 23.4° positions of 2Θ (reflections (100) and (010), respectively) as expected for nylon 11.[45] The presence of these well-resolved peaks is typical for

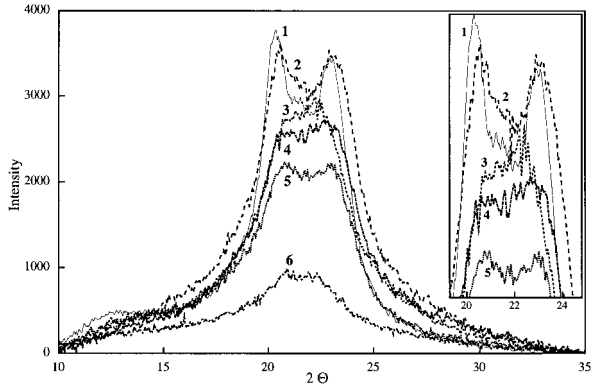

Figure 12 X-ray diffraction curves of: (1) nylon 11 powder, nylon 11 D-60 coatings containing nominal 15 vol % of: (2) carbon black, (3) hydrophobic silica, (4) silanated silica; (5) 0% filler, (6) amorphous nylon 11 D-60.

crystalline nylon with the triclinic α-form of crystal structure. There was also a particulate scattering pattern from the powder present at $2\Theta = 7°$, which was virtually absent from the X-ray curve of the sprayed coatings due to the deformation of the powder during spraying. Suppression of the X-ray peaks was observed for all sprayed coatings compared to nylon 11 powder, with the largest drop in the case of unfilled nylon 11 coatings, which indicated the lowest crystallinity content of the unfilled coatings. An increased amount of filler resulted in increases in the height of the peaks and in the overall areas under the curves, likely due to the filler initiated crystallization. For all composite coatings, a fusing of two peaks was also observed. Shifting of the (010) peak to a lower angle corresponded to a larger spacing between hydrogen-bonded sheets of nylon main chains, indicating a decreasing crystalline perfection and transition to the pseudohexagonal δ phase of the nylon matrix.[45]

No cracking or shrinkage was observed in the coatings due to crystallization. It was hypothesized that because of the space restriction imposed by the nanosized filler, the crystalline domains were small and perhaps concentrated in the vicinity of the particles and, therefore, did not cause significant volume shrinkage in the coatings.

The results from X-ray analysis are summarized in Figure 13 for all sprayed coatings, presented as an increase in fractional crystallinity of nanocomposite coatings relative to the crystallinity content of a pure nylon 11 D-60 coating. The crystallinity content increased with the addition of nanosized fillers, in agreement with the trends shown by DSC analysis. Hydrophobic silica and carbon black reinforced coatings containing nominal 15 vol % of filler exhibited the largest fractional crystallinity increase, determined to be 15.2 and 9.9% increases over pure nylon 11 D-60 coatings, respectively. Using this methodology, again assuming the crystallinity content of the pure polymer powder (nylon 11 D-60) to be 21%, this implied 19 and 12% absolute crystallinity content in these sprayed nanocomposites, respectively, while 15 vol % silanated silica filled coatings exhibited a 9% increase in crystallinity content.

Crystallinity increases were always higher in hydrophobic silica than in hydrophilic silica-filled nylon 11, and the highest values of crystallinity were measured in carbon black-filled samples. In D-30 samples the differences in crystallinity contents were not significant between nominal 10 and 15 vol % filler contents for either filler type.

The variations in crystallinity between different silicas and carbon black confirmed that the filler presence and its content played a significant role in the polymer crystallization during coating deposition, either through changes in thermal input or due to nucleation phenomena or liquid constraint. The clear differences in the crystallinity content between the D-30 and D-60 composite coatings with the same filler content indicated that along with the filler effects, the degree of heating of the polymer particles in flight and also the substrate temperature profile, including the preheating of the substrate necessary for obtaining coatings, could significantly contribute to the degree of crystallinity achieved in thermal

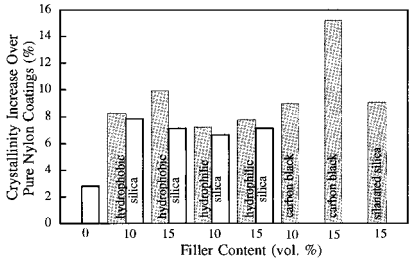

Figure 13 Fractional crystallinity increase of filled nanocomposite coatings relative to pure sprayed nylon 11 D-60 coatings as a function of a filler type and content (as determined by X-ray analysis). White and gray bars represent nylon 11 D-30 and D-60, respectively.

sprayed coatings. Further study will be required to separate and quantify the various contributors to polymer crystallization.

CONCLUSIONS

Nano-sized silica and carbon black-filled nylon 11 coatings were successfully sprayed using the HVOF combustion spray deposition process. Spraying parameters were sufficiently optimized so that the polymer particles were well splatted on impact at the substrate. FTIR analysis confirmed that the optimal HVOF spraying parameters did not result in significant degradation of the starting polymers. In the coatings produced using nylon 11 D-30, particle size 30 μm, well-splatted particles, and fine or no-cell structure was observed, corresponding to better spatial filler distribution in the polymer matrix. Silane treatment of silica particles reduced silica particle agglomeration and improved silica dispersion in the final coatings.

Thermal sprayed nanocomposite nylon 11 coatings had higher crystallinity contents than the pure nylon 11 coatings. It was believed that the filler acted as a nucleation site, promoting crystallization and, therefore, increased crystallinity. Coatings produced from smaller polymer powder particle size (D-30) typically had lower crystallinity contents than coatings produced from larger polymer particle sizes (D-60) with corresponding filler contents. Hydrophobic silica and carbon black-filled coatings exhibited higher crystallinity increases than hydrophilic silica-filled coatings for both D-30 and D-60 powders. Coatings produced from smaller particle sizes were denser and showed lower porosity contents than coatings produced from larger polymer particle sizes. It is believed that smaller polymer particles were heated more homogeneously, and more thoroughly melted, during processing, resulting in improved flow on impact at the substrate. Also, because of the lower crystallinity content of D-30 coatings, higher densities were believed to be the result of lower porosity content in these coatings.

This material is based upon work supported by the National Science Foundation under Grant No. 9713650. The authors would also like to thank Elf Atochem North America, Inc. and Degussa Corporation for the donation of powders, and Stellite Coatings for donation of the 0.076 m nozzle used for this work. The authors greatly appreciate assistance by Mr. Don Gentner during thermal spraying and Mr. David van Rohr during SEM analysis.

REFERENCES

1. Misev, T.A. Powder Coatings: Chemistry and Technology; John Wiley & Sons: New York, 1991.
2. Sumita, M.; Shizuma, T.; Miyasaka, K.; Ishikawa, K. J Macromol Sci Phys 1983, B22, 601.
3. Sumita, M.; Tsukumo, T.; Miyasaka, K.; Ishikawa, K. J Mater Sci 1983, 18, 1758.
4. Messersmith, P. B.; Giannelis, E. P. Chem Mater 1994, 6, 1719; J Polym Sci A Polym Chem 1995, 33, 1047.
5. Yano, K.; Usuki, A.; Okada, A.; Kurauchi, T.; Kamigaito, O. Polym Prep 1991, 32, 65.
6. Kumar, V.; Erwin, L. Antec'87, 1987, 152.
7. Giannelis, E.P. Adv Mater, 1996, 8, 29.
8. Fender, T.D. Mat Technol, 1996, 11, 16.
9. Brogan, J. A., Ph.D. Dissertation, State University of New York, Stony Brook, NY (1996).
10. Liao, H.; Beche, E.; Berger, F.; Coddet, C. Proc 15th Int'l Therm Spray Conf, Nice, France, ASM International®, Materials Park, OH, 1998, p. 25.
11. Lugscheider, E.; Herbst, C.; Fischer, A. Proc 15th Int'l Therm Spray Conf, Nice, France, ASM International®, Materials Park, OH, 1998, p. 19.
12. Borisov, Y.; Korzhik, V.; Sviridova, I.; Skorokhod, A. Proc 1st United Therm Spray Conf, Indianapolis, ASM International®, Materials Park, OH, 1997, p. 239.
13. Lima, R. S.; Takimi, A. S.; Lima, M. D.; Bergmann, C. P. Proc 1st United Therm Spray Conf, Indianapolis, IN, ASM International®, Materials Park, OH, 1997, p. 215.
14. Varacalle, D. J., Jr.; Couch, K. W.; Budinger, V. S. Proc Int'l Therm Spray Conf, Cinncinati, OH, ASM International®, Materials Park, OH, 1996, p. 251.
15. Sweet, G. K. Proc 5th Nat Therm Spray Conf, Anaheim, CA, ASM International®, Materials Park, Ohio, 1993, p. 381.
16. Bristowe, W.W. Proc Conf on Composites Manufacturing and Tooling'94, Anaheim, CA, sME Technical Paper, EM94–116/1-16, 1994.
17. Brogan, J. A.; Berndt, C. C., J Mater Sci, 1997, 32, 2099.
18. Skorokhod, A. Z.; Pisanova, E. V.; Zhandarov, S. F.; Yurkevich, O. R. J Appl Polym Sci 1995, 57, 1263.
19. Bao, Y.; Gawne, D. T. Surface Eng 1995, 11, 215.
20. Zhang, T.; Gawne, D. T.; Bao, Y. Proc 1st United Therm Spray Conf, Indianapolis, IN, ASM International®, Materials Park, OH, 1997, p. 231.
21. Bao, Y.; Gawne, D. T. Proc 9th Int'l Therm Spray Conf, Cinncinati, OH, ASM International®, Materials Park, OH, 1996, p. 227.

22. Brogan, J. A.; Berndt, C. C.; Claudon, A.; Coddet, C. Proc 15th Int'l Therm Spray Conf, Nice, France, ASM International®, Materials Park, OH, 1998, p. 1173.
23. Tufa, K.Y.; Gitzhofer, F. Proc 1st United Therm Spray Conf, Indianapolis, IN, ASM International®, Materials Park, OH, 1997, p. 223.
24. Henne, R. H., Schitter, C. Proc 8th Nat Therm Spray Conf, Houston, Texas, ASM International;, Materials Park, Ohio, 1995, p. 527.
25. Bao, Y.; Gawne, D. T. J Mater Sci, 1994, 29, 1051.
26. Kawase, R., Nakano, A. Proc 9th Int'l Therm Spray Conf, Cinncinati, OH, ASM International®, Materials Park, OH, 1996, p. 257.
27. Schadler, L. S.; Laul, K. O.; Smith, R. W.; Petrovicova, E. J Therm Spray Technol, 1997, 6, 475.
28. Irving, B.; Knight, R.; Smith, R. W. Welding J 1993, 72, 25.
29. Blackmore, C. E. Finishing 1990, 14, 44.
30. Vogdes, Ch. Plastics Eng 38, 33, 1983.
31. Kohan, M. I. Nylon Plastics, SPE Monograph; John Wiley & Sons: New York, 1973.
32. Balard, H.; Papirer, E. Prog Organic Coatings 1993, 22, 1.
33. Novakoski, D.; Juengel, R.; Laube, S. Rubber Plastic News 1996, 26, 39.
34. Wypych, G. Fillers; ChemTech Publishing: Toronto, 1993.
35. Schut, J. H. Plastics World 1995, 53, 61.
36. Plueddemann, E. P. Silane Coupling Agents; Plenum Press: New York, 1982.
37. Chomiak, J. Combustion. A Study in Theory, Fact and Application; Abacus Press: New York, 1990, p. 446.
38. Annual Book of ASTM Standards, ASTM D 792-91, Vol. 08.01; ASTM: Philadelphia, PA, 1991.
39. Cullity, B. D. Elements of X-ray Diffraction; Addison–Wesley: Reading, MA, 1978, p. 284.
40. Kreye, H.; Zimmermann, S.; Heinrich, P. Proc 14th Int'l Therm Spray Conf, Kobe, Japan, ASM International®, Materials Park, OH, 1995, p. 393.
41. Svoboda, M.; Schneider, B.; Stokr, J. Collect Czech Chem Commun 1991, 56, 1461.
42. Bao, Y.; Gawne, D. T.; Vesely, D.; Bevis, M. J. Surface Eng 1994, 10, 307.
43. Scott, K. T.; Kingswell, R. In Advanced Surface Coatings; Rickerby D.S.; Mathews, A., Eds.; Chapman and Hall: New York, 1991, p. 217.
44. Geil, P. H. Polymer Single Crystals; R. E. Krieger Publishing Co., Inc.: Hungtington, NY, 1973.
45. Chen, P. K.; Newman, B. A.; Scheinbeim, J. I.; Pae, K. D. J Mater Sci 1985, 20, 1753.